Gravity Waves above Propagating Tropopause Depressions - Idealized Numerical Simulations

Michael Binder

University Innsbruck

Advisors:

Dr. Andreas Dörnbrack (DLR)

Dr. Bernd Kaifler (DLR)

Assoc. Prof. Alexander Gohm

July 11, 2021

Abstract

This proposal introduces the Master's thesis on gravity waves (GWs) above propagating tropopause depressions by describing its motivation and the planned methods to approach the topic. The excitation of GWs above tropopause depressions is a proposed non-orographic GW source that could explain important GW observations in the southern hemisphere winter stratosphere above the Southern Ocean. After clarifying the relevance and potential of the mechanism, planned idealized simulations with the EULAG model are explained. To avoid over-complicated simulations with complex results, possible simplifications for first simulations have been identified. It is the goal of this thesis to provide first answers on the relevance of the mechanism and a good baseline for final complex simulations.

1. Introduction

The essential role of atmospheric gravity waves (GWs) within the Earth's climate and its impact on atmospheric circulations is well-known for years (Fritts, 2003). They affect the dynamics and physics of the atmosphere on a wide range from turbulent to planetary scales (Plougonven et al., 2020 and Williams et al., 2017). The proposed Master's thesis is based on a recent paper by Dörnbrack et al. (2021) who suggest the excitation of GWs above propagating tropopause depressions (TDs). This mechanism could play an important role in the southern hemisphere and explain observations of GWs in the stratosphere in a region around 60°S above the Southern Ocean, where other sources like topography are unlikely (Hindley et al., 2020).

Considering the extensive background that comes along with this thesis its motivation and goal is split into five subsections. Subsequently follows a description of the planned methods (section 3) and tools (section 4) to approach the topic. A timetable concludes the proposal.

2. Motivation and Goal

2.1. Atmospheric GWs and their representation in general circulation models

The atmosphere above the boundary layer is almost constantly characterized by a positive static stability. In this stably stratified part of the atmosphere vertically displaced air parcels experience a restoring force predominately caused by buoyancy which enables the excitation and propagation of internal GWs. These oscillations in the atmosphere are observable through perturbations in the atmosphere's wind, temperature, density and pressure fields and they appear at a wide range of horizontal wavelengths from ≈1 km, where the waves are non-hydrostatic, to ≈10 km, where they are approximately hydrostatic, through to ≈100 km, where rotation of the Earth becomes important (inertia-gravity waves), up to ≈1000 km, where the variation of the Coriolis parameter with latitude must be taken into account (Rossby-gravity waves) (Teixeira, 2014 and Gill, 1982).

Excited primarily by orography in the troposphere, GWs can propagate horizontally and

vertically. When propagating upwards, GWs grow in amplitude due to a decreasing density with height and ultimately break as they reach a critical region in the atmosphere, dissipate energy and affect the general circulation by depositing momentum. This can happen far away from the wave's source region (Teixeira, 2014 and Eliassen and Palm, 1960). However, critical regions or layers in the atmosphere vary for different vertical wavelengths and define themselves through the fluid's stratification and background wind (Teixeira, 2014). Furthermore, their effect on the propagation of GWs can be a lot more diverse and also lead to (partial) wave reflection and, so-called, wave trapping (Fritts et al., 2018 and Scorer, 1949), resulting in a vast and manifold forcing on the atmosphere's general circulation (Alexander et al., 2010).
State-of-the-art general circulation models (GCMs) are not yet capable of resolving this full range of effects how GWs impact the atmospheric flow. This is not expected to change within the near future as physical limits in hardware development also start to constrain further advances in computational climate science (Balaji, 2021 and Balaji, 2015). Thus, representing horizontal or vertical wavelengths of just a few kilometers is one challenge, but covering the nonlinear processes related to wave breaking at scales much smaller than the wavelength is another. Furthermore, the sources of GWs include processes that are poorly resolved by GCMs themselves like fine-scale topography, convective heating, localized shear zones or frontal structures (Medvedev and Yiğit, 2019, Fritts, 2003 and Plougonven and Zhang, 2014).

As a result, parameterizations have to account for the significant portion of subgrid-scale processes. Since the main feature of GWs is the transport of horizontal momentum upward into the middle and upper atmosphere, most GW parameterisations are based on two assumptions. Firstly, GWs are excited within the troposphere and, secondly, they only propagate vertically (Plougonven et al., 2020 and Alexander et al., 2010). Physically based parameterisations of waves from non-orographic sources exist (e.g. Scinocca, 2003), but lack observational constraints (Plougonven and Zhang, 2014) and are restricted to the troposphere. Sources in the upper atmosphere like secondary generation or the proposed mechanism of Dörnbrack et al. (2021) are not represented (Plougonven et al., 2020 and Kim et al., 2003).

The simplified columnar propagation of GWs has its advantage within the constraints of parallel computing, but multiple studies already showed that waves can propagate horizontally due to the refraction of jet streams and/or advection of the mean wind, too (Dunkerton, 1984, Preusse et al., 2002, Sato et al., 2009, Sato et al., 2012 and Ehard et al., 2017).

It follows that continued improvements of GW parameterisations are of great interest as long as resolution limits the dynamics of global numerical models. Recent approaches incorporating deep learning with neural networks (Matsuoka et al., 2020) principally allow for horizontal propagation of sub-grid scale waves at a reasonable computational cost. First results are promising, but it is still difficult to predict, if this recent trend marks the next generation of parameterisations ("Soft AI" approach) or even replaces larger parts within weather and climate predictions as discussed by Chantry et al. (2021) who refer to it as "Medium AI" and "Hard AI" approaches.

Either way, it does not mitigate the importance of expanding our knowledge on the underlying processes by which GWs affect the atmosphere and this is the goal of the proposed thesis. An improved understanding of ongoing mechanisms could advance parameterizations and maybe contribute to the explanation of GW observations whose origins are not fully understood today. Probably the most significant of these observations is the one of interest for the proposed thesis, too. It is discussed in detail in the next section.

2.2. The gravity wave belt around 60°S and the cold pole problem

The increasing number of GW observations from satellites (Hindley et al., 2019, 2020), ground-based lidar systems (N. Kaifler et al., 2020 and B. Kaifler and Kaifler, 2021), aircraft (Rapp et al., 2021 and Fritts et al., 2016) and balloons (Plougonven et al., 2013) help to constrain GW parameterisations, but also reveal their deficiencies and point out gaps in

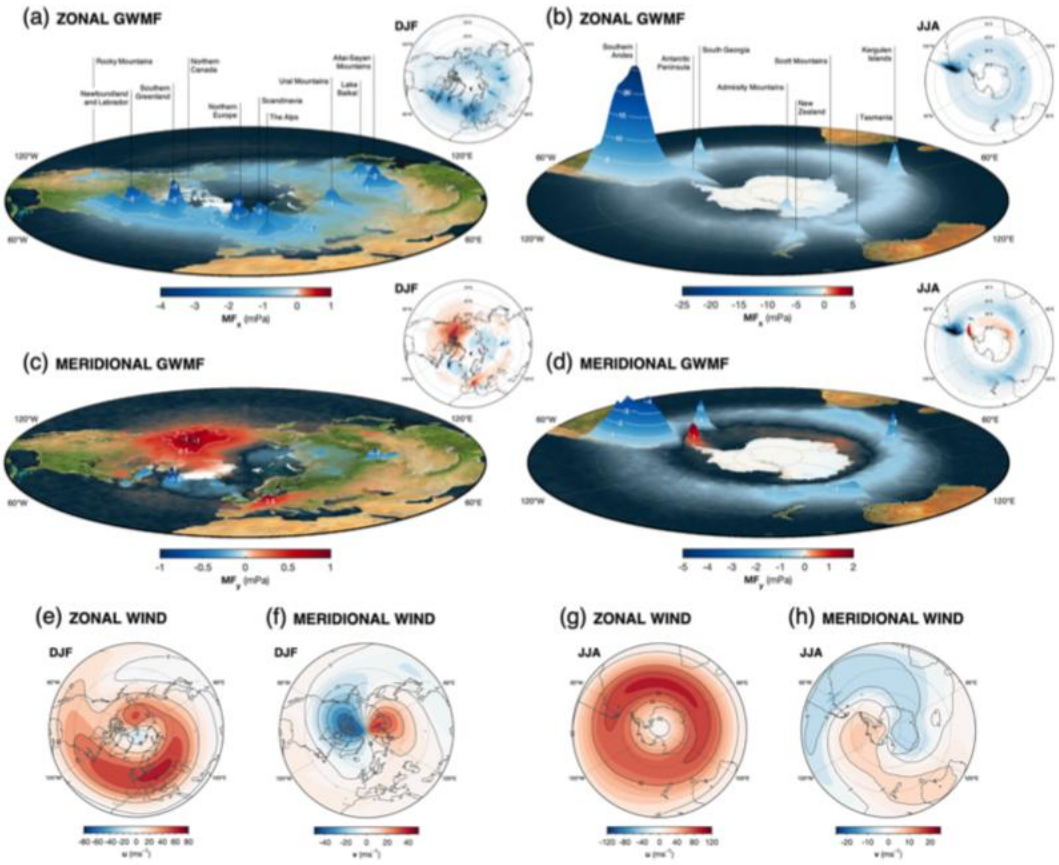

Figure 1: Stereographic maps of average wintertime zonal (a, b) and meridional (c, d) GWMF near 40 km altitude derived from AIRS/Aqua 3-D satellite observations for the period 2002–2019. Winter is defined as December–February (June–August) for the Northern (Southern) Hemisphere. GWMF values that are close to zero have been made transparent to reveal the surface features below, and landmarks that lie beneath regions of increased GWMF have been labeled. Inset in the top right of each panel is a stereographic map of the same data but centered on the north and south poles. These inset panels share a color scale with the corresponding 3-D contours. Panels (e)–(h) show average wintertime zonal and meridional winds at 3 hPa for the period 2002–2019 from ERA5 reanalysis. Taken from Hindley et al., 2020.

our current theoretical knowledge on GWs. A phenomenon that was already visible in observations by Wu and Waters (1996), but still lacks a conclusive explanation, is a GW belt around 60 °S during the austral winter. It is visualized in parts b and d of Fig. 1 from Hindley et al. (2020) who provide an extensive overview on seasonally averaged multi-year gravity wave momentum flux (GWMF) derived from satellite observations.

Orography undoubtedly leads to the GW hot spot between 55°W and 80°W above the southern Andes and the Antarctic Peninsula, but it only contributes about 25% to the total GWMF within the latitude band from 35°S to 68°S as stated by Hindley et al. (2020). Following Sato et al. (2012) and accounting for a far downstream propagation of GWs excited by the Andes, the observable GWMF in the East of the defined longitude region could be allocated to this predominantly local source, too. However, this does not heavily affect the argument of Hindley et al. (2020) that about 75% of zonal and meridional GWMF are observed at remaining longitudes over the Southern Ocean mostly peaking around 60°S (Hindley et al., 2020).

It has been shown that small, mountainous islands contribute to this oceanic GWMF (Garfinkel and Oman, 2018; McLandress et

al., 2012, Alexander et al., 2009), but again they only result in local peaks as indicated in Fig. 1b. So non-orographic origins of GWs are most likely the reason for the widespread, belt-like structure of the GWMF (Hendricks et al., 2014). Jet streams and fronts most likely contribute to the observed momentum flux (Plougonven and Zhang, 2014 and Hendricks et al., 2014) and have also been investigated on the basis of idealized simulations (O'Sullivan and Dunkerton, 1995). Polichtchouk et al. (2018) analysed the sensitivity of high-resolution atmospheric models to non-orographic GW parameterisations and concluded a significant dependence in the same manner as Choi and Chun (2013) showed that convective gravity wave drag parameterisations (a specific non-orographic source) can have a significant influence on global climate models. In addition, Jewtoukoff et al. (2015) were able to assign wave signatures in their balloon observations to non-orographic sources, but so far none of the discussed mechanisms provides a comprehensive explanation of the wide spread observation of GWs over the Southern Ocean in the austral winter and it is still possible that some important mechanisms have not yet been considered.

The gravity wave belt around 60°S gained crucial relevance since McLandress et al. (2012) suggested its connection to the longstanding cold pole problem found in nearly all modern GCMs and chemistry climate models (CCMs). During the southern hemisphere winter months a polar vortex or polar night jet (PNJ) develops around 60°S high up in the stratosphere characterized by strong zonal westerly winds. GCMs and CCMs overestimate this PNJ, which also entails lower stratospheric temperatures over the pole compared to observations (Butchart et al., 2011, Geller et al., 2013 and Eyring et al., 2010). As a result, the polar vortex breaks down too late in the spring with significant consequences on, for example, the simulated ozone trends in the Antarctic middle stratosphere (Stolarski et al., 2006). The Antarctic ozone hole persists too long into the late spring and since Antarctic ozone depletion is the primary driver of recent southern hemisphere summertime climate change (e.g. Arblaster and Meehl, 2006), a delay in the vortex breakdown impacts the timing of the simulated tropospheric response.

McLandress et al. (2012) showed through their simulations that missing gravity wave drag from parameterisations can explain this substantial zonal wind bias around 60°S and the directly related "cold pole". A deeper understanding of the key processes that lead to the observed gravity wave belt during the austral winter could significantly improve GW parameterisations and ultimately improve long-term climate predictions through more realistic and robust GCMs.

2.3. The excitation of GWs above tropopause depressions

As outlined in the previous section, non-orographic GW sources have already been investigated from various perspectives, but are not yet able to fully explain the consistent, wide-spread appearance of GWs around 60°S. Based on observations and the analysis of high-resolution ERA5 data, Dörnbrack et al. (2021) are currently proposing a new mechanism that has the potential to fill this gap. They suggest the excitation of GWs above tropopause depressions (TDs) in the stratosphere just like they would appear above surface obstacles in the troposphere.

Though various definitions of the tropopause exist, all rely on abrupt changes in physical or chemical properties when transitioning from a weakly stratified troposphere ($N^2 \approx 1{\cdot}10^{-4}\mathrm{s}^{-2}$) to a comparatively strongly stratified stratosphere ($N^2 \approx 4{\cdot}10^{-4}\mathrm{s}^{-2}$; Birner, 2006). Common definitions are based on the thermal stratification (negative temperature lapse rate in the troposphere, positive lapse rate in the stratosphere; WMO, 1957), refer to the dynamical tropopause using Ertel's potential vorticity (WMO, 1986) or rely on chemical tracers like ozone. Despite fundamental differences in those approaches, each supports the simplification of treating the tropopause as an impermeable boundary, which is definitely not true, but a good approximation for idealized investigations.

In the vicinity of jet streams or upper level frontal zones and associated with baroclinic processes the extratropical tropopause now experiences deflections or even undergoes a

folding process as visualized in Fig. 2. Dry stratospheric air penetrates down into the troposphere and folds underneath the warm air towards the equator (here northward for southern hemisphere) for deep depressions. The shape of the TD and especially the vertical extend of the prominent tongue of stratospheric air can vary significantly depending on the large scale flow conditions and strength of the upper level frontal system. This has already been discussed extensively from an observational (e.g. Shapiro, 1978 and Keyser and Shapiro, 1986) and model (Škerlak et al., 2015) perspective. Fortunately, the excitation of GWs above such a depression might not be very sensitive to the fold's shape far below the tropopause. Isentropes, that are deflected downwards, but rise again on the other side of the depression (e.g. 360-390 K in Fig. 2a) are much more interesting for the proposed mechanism considering its similarity to flow over orography. Additionally, the zonal shape of the depression is more relevant for the GW forcing. This alongstream cross section (orthogonal on 2a) was rarely discussed in relevant publications, since the main folding process happens in the cross-stream direction. Based on the ERA5 case study conducted by Dörnbrack et al. (2021) (Fig. 3), the zonal width at half maximum of the propagating TD can be estimated between 4° and 8° in zonal direction, which transfers to $a = 240{-}480\,\mathrm{km}$ ($1° \approx 63\,\mathrm{km}$ at 55°S).

Following estimates based on idealized scenarios (constant background wind U and Brunt–Väisälä frequency N) such 'mountain widths' are expected to excite waves within the hydrostatic regime. Towards the wider end of a the advection time for an air parcel to pass over the mountain $\tau_a = \frac{a}{U}$ is even comparable in magnitude to the period of inertial oscillation due to Earth's rotation ($\tau_f = \frac{2\pi}{f}$) with the Coriolis parameter $f \approx 10^{-4}\mathrm{s}^{-1}$ for mid-latitudes. So the Rossby number

$$Ro = \frac{U}{fa} \approx \frac{\tau_f}{\tau_a} \approx 2\pi \qquad (1)$$

is close to $O(1)$ and Coriolis forces can no longer be neglected. Together with the buoyancy forces they act together as restoring forces resulting in both horizontal and vertical oscillations, which are called hydrostatic inertia-gravity waves (e.g. Gill, 1982 and Lin, 2007).

A major difference of potential GWs above TDs to classic mountain waves is the transient nature of their source. Pfister et al. (1993) already investigated the propagation of waves in the stratosphere due to a transient forcing by exposing the background flow to a time-varying obstacle, but only lifted and receded the bottom of the stratosphere. A tropopause fold travels eastward with the phase speed of the Rossby wave, so the relative motion of the stratospheric air aloft with respect to the propagation of the fold is responsible for the excitation of the GWs. The increasing wind speed with height due to the PNJ, which is already important for the propagation of the waves, is, therefore, important for their excitation, too.

2.4. The propagation of GWs above tropopause depressions

Considering the hydrostatic nature of GWs excited by TDs, the strongest wave signal should more or less appear directly above a propagating depression. In fact, Dörnbrack et al. (2021) observed exactly this feature in ERA5 data (Fig. 3), when analysing lidar measurements from DEEPWAVE research flight 25. Clear wave signals are observed directly above the tropopause fold for multiple points in time. This inspires confidence in the proposed mechanism and suggests that GWs can be observed along the whole path of the baroclinic system responsible for the depression. Now, the last piece to the puzzle for explaining the wave belt above the Southern Ocean during the austral winter in Fig. 1b and 1d is the meridional propagation of GWs in the stratosphere. This is important, because especially in the southern hemisphere pronounced frontal systems are not deviating significantly from a latitude band around 50°S (Škerlak et al., 2015) though GWs are observed frequently further south.

Two mechanisms are at hand concerning this meridional propagation. At first, the orientation of the TDs is rarely exactly North-South resulting in an inclined wave vector with respect to the predominantly westerly flow in the upper stratosphere. The wave vector defines the propagation direction, so this mechanism is always present and relevant as soon as tilted obstacles are in place as discussed by Preusse

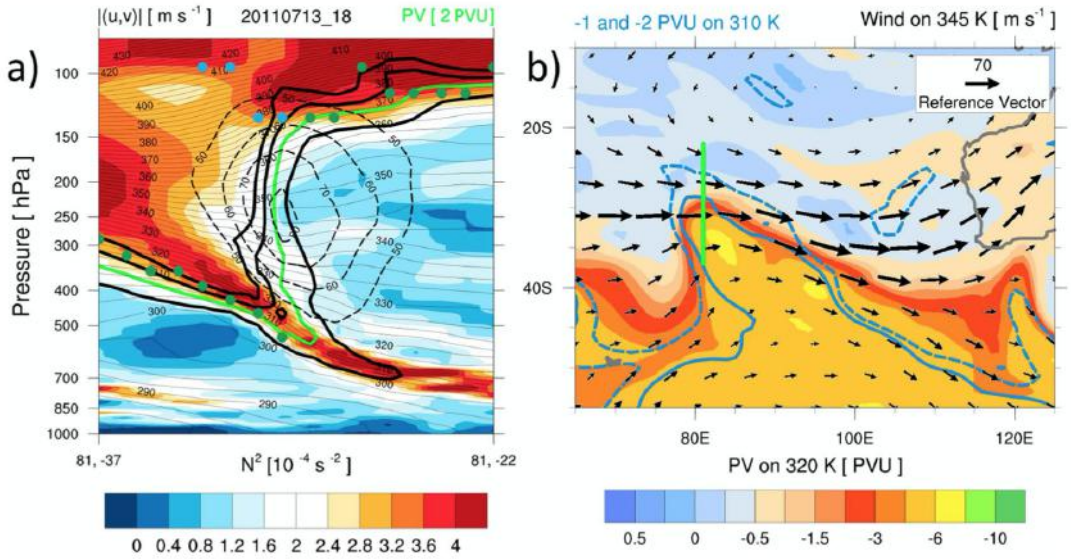

Figure 2: Example of a deep tropopause fold near the subtropical jet west of Australia at 18 UTC on 13 July 2011. The vertical cross section shown in Figure 2a is aligned along 81°E from 37S° to 22°S (green line segment in Figure 2b). Displayed are (a) the squared Brunt-Vaisala frequency (N^2, colored), potential vorticity (-1 to -4 PVU, thick solid lines, -2 PVU in green, rest in black), the WMO first and second tropopauses (green and blue solid circles, respectively), horizontal wind speed (in $1\,\mathrm{ms}^{-1}$, dashed contours), and isentropes (in K, thin contours) and (b) PV on 320 K (colored, in PVU), contours of PV on 310 K at -1 PVU and -2 PVU (dashed and solid blue, respectively), and horizontal wind speed on 345K (reference vector in the top right, in $1\,\mathrm{ms}^{-1}$). The West Coast of Australia is visible as grey contour. Taken from Škerlak et al., 2015.

et al. (2002) for GWs excited by the Andes at similar latitudes. The second process is based on ray-tracing theory and was first discussed and applied by Dunkerton (1984). It describes the modification of the meridional (horizontal) wavenumber by the background wind field with

$$\frac{dl}{dt} = -(k\frac{\partial U}{\partial y} + l\frac{\partial V}{\partial y} + \frac{\beta f}{\hat{\omega}}) \approx -k\frac{\partial U}{\partial y}. \quad (2)$$

In a simplified scenario the time rate of change of the meridional wavenumber l along the ray is proportional to the meridional gradient of the background wind U and the zonal wavenumber k. In other words, horizontal wind shear develops a meridional component of the wave vector even in the case of a purely zonal initial propagation. In general, this phenomenon leads to a refraction of internal GWs into the southern hemispheric PNJ at 60°S, which has already been described by a number of publications (e.g. Dunkerton, 1984, Preusse et al., 2002, Sato et al., 2009, Sato et al., 2012, Ehard et al., 2017 and Jiang et al., 2019). Jiang et al. (2019) further add, that waves are elongated towards the stronger background wind (towards the center of the PNJ) and shortened on the opposite side with weaker winds.

2.5. Research goals

In the end, both described mechanisms play an important role for the meridional propagation of GWs. Together with the regular appearance of Rossby wave trains (baroclinic systems involving TDs) at middle latitudes in the southern hemisphere, these processes could provide a conclusive explanation for the widespread and patchy stratospheric GW activity all the way around the Southern Ocean shown in Fig. 1b and 1d. It is the goal of the proposed thesis to further investigate the relevant processes related to GWs above tropopause depressions through idealized simulations and eventually provide first answers on its relevance for explaining the discussed GW belt above the Southern Ocean. More specifically, the Master's thesis shall answer the following research questions:

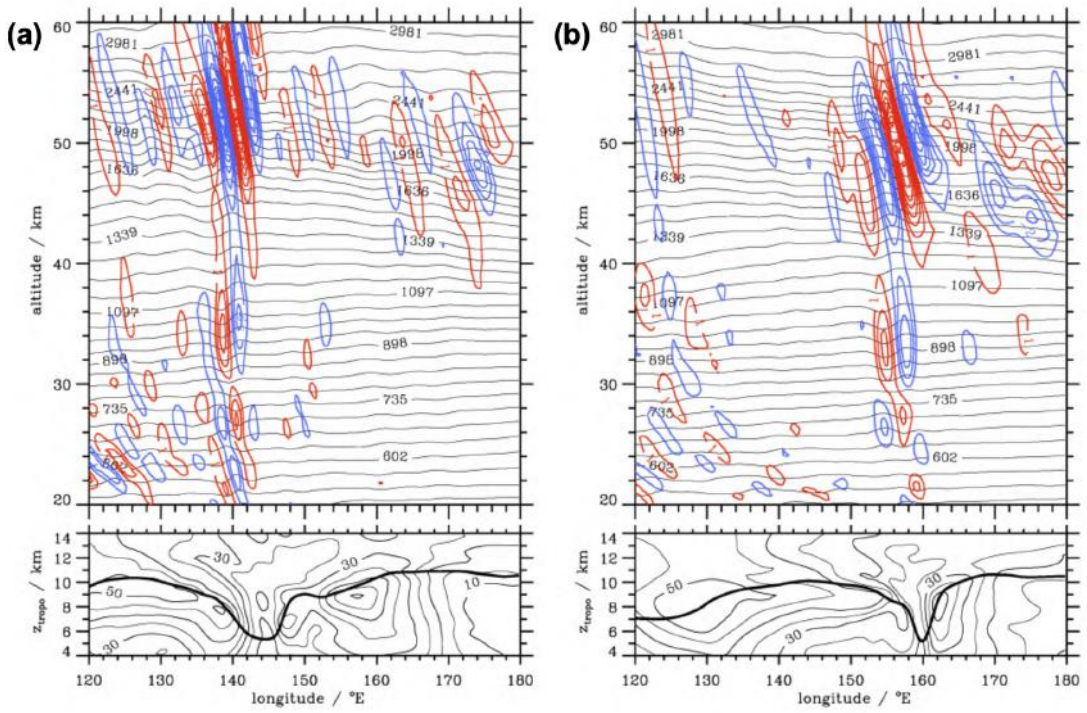

Figure 3: Temperature perturbations (K, red and blue contour lines) and potential temperature (K, black lines in logarithmic scaling) along 55°S on 17 July 2014 15 UTC (a) and 18 July 2014 09 UTC (b). The bottom panels depict the height of the dynamical tropopause (thick black lines, meridional average from 52.5°S to 57.5°S) and the horizontal wind (ms^{-1}, thin black lines) at the same instances. Data: One hourly ERA5 data. Taken from Dörnbrack et al. (2021).

1. How sensitive is the excitation and propagation of GWs above TDs to the shape of the depression (depth, width, asymmetry)?
2. Which wave regimes are present above propagating TDs and what wavelengths and amplitudes do we expect?
3. What is the contribution of a tilted TD (leading to an inclined wave vector) to a meridional propagation of GWs?
4. What is the contribution of horizontal wind shear in the stratosphere to a meridional propagation of GWs?

3. Methods

The goal of this thesis is an improved understanding of the processes that lead to observed gravity waves above TDs. A complete three dimensional simulation of the troposphere and stratosphere including all relevant features, more precisely a Rossby wave train and jet stream at the tropopause and a PNJ higher up in the stratosphere to the south, requires challenging initial conditions to obtain suited fields of wind, temperature and pressure (compare section 3.4). Though such a simulation has to be the final step to prove or debunk the described mechanisms, preliminary investigations of simplified simulations likely provide first insights and might significantly help to setup and interpret more complex runs. Therefore, the proposed thesis comprises a selection of simulations with reduced complexity to address parts of the problem step by step.

The fundamental simplification for all preliminary simulations is the focus on dynamics in the stratosphere by introducing the tropopause as the lower boundary of the simulation's domain. It is clear that the tropopause is not an impermeable surface, but observations from radiosondes (Birner et al., 2002 and Birner, 2006) and GPS data (Randel et al., 2007) revealed a significantly higher thermal

stability of the extratropical tropopause inversion layer compared to model and reanalysis data. This higher stratification further inhibits troposphere-stratosphere exchange at the tropopause and justifies the approach of using the tropopause as the lower boundary for first simulations. The planned simulations and corresponding simplifications are described in the following subsections and summarized in table 1.

3.1. Model setup and verification

Simulations 2D001-2D004 of table 1 ensure that the model is setup correctly and provides physically reasonable outputs. In that sense, it is the goal to reproduce some fundamental analytic results based on linear theory with nonlinear EULAG simulations. Queney (1948) was the first to summarize different flow regimes over mountains based on the method of small adiabatic perturbations. His results can be compared to simulations from a visual perspective by looking at the perturbations and fluxes in the atmosphere and from a mathematical one by comparing the wave drag

$$\mathcal{F} = \int p' \frac{\partial h}{\partial x} dx \tag{3}$$

to its analytic solution in a linear framework (Gill, 1982). Assuming an impermeable tropopause at the lower boundary of the simulations results in a TD that acts like a flipped mountain (valley) on the stratosphere, so a comparison of our model to Queney's solutions for different mountain wave regimes (nonhydrostatic, hydrostatic, inertia-gravity) provides a reasonable baseline and validation of the model for the planned simulations.

Depending on the application or numerical problem at hand, the function, that describes the surface boundary (mountain shape) can have useful or disturbing properties. The Witch of Agnesi

$$h_{Agnesi}(x) = \frac{h_0}{(\frac{x}{a})^2 + 1} \tag{4}$$

used by Queney (1948) is a convenient equation of the terrain height for analytical analysis, but it is non-zero for the whole domain of discrete simulations. In the case of a transient lower boundary this effect leads to inconsistent boundary conditions at the horizontal borders, making this a less appropriate shape for a propagating TD. A suitable alternative is a $1+cos(\pi\phi)$ function. It drops to 0 for $|\phi| = 1$. With

$$h_{cos}(\phi) = \frac{h_0}{16}(1 + cos(\pi\phi))^4 \tag{5}$$

and $\phi = \frac{x}{4a}$ Epifanio and Durran (2001) used a variation of this function, which is more comparable to the Witch of Agnesi (4). Setting $h_{cos}(\phi) = 0$ for all grid points $|x| > 4a$ results in a continuous and differential lower boundary that does not interfere with horizontal boundary conditions as long as the mountain or depression is not too close to the edges. Furthermore, all contributions to the surface pressure drag are confined to a small neighbourhood around the mountain peak. Metz and Durran (2021) state that the wave drag is a factor 1.3 higher compared to the Witch of Agnesi, but further comparisons of the terrain functions and their impact on the overlying flow are carried out (simulation 2D002).

In simulations 2D003 it is the goal to observe the propagation of waves for a rising and for a moving lower boundary in an atmosphere at rest. With no background wind and a constant static stability the simulation is expected to mimic the perturbations in a water tank, when for example pulling an obstacle at the bottom through the quiescent fluid. Furthermore, in this way the linearized governing equations simplify even further and it might be possible to identify patterns in the waves' group (c_g) and phase velocities, which are characteristic for the scenario without a background flow. For example the parallel orientation of c_g to the wave's phase lines and the corresponding direction of the energy propagation (Lin, 2007).

For a last physical validation it is appropriate to start two-dimensional simulations of a transient TD by reproducing the simulations of a zonally oscillating TD conducted by Prusa and Smolarkiewicz (2003) (simulation 2D004 in table 1). They showed that inertia-gravity waves are constantly observable above a TD (h_0=500 m, a=200 km) for a constant stratospheric background wind of $10\,\mathrm{m\,s^{-1}}$, a constant buoyancy frequency N of $0.02\,\mathrm{s^{-1}}$ and an isothermal stratosphere. However, the waves above the TD are expected to change continu-

Table 1: EULAG simulation runs

	Simulation	Description
2D	001: Fundamental flow regimes over orography	- Non-hydrostatic wave regime - Hydrostatic wave regime - Inertia-gravity wave regime
	002: Mtn / TD shape comparison	- Witch of Agnesi - $(1+cos(\phi))$ shape - $(1+cos(\phi))^4$ shape
	003: Transient lower boundary test	- Mtn rises or moves in x-direction - No background wind - Test smooth start up / end of motion
	004: Transient TD like Prusa et al. (2003)	- Oscillating TD in zonal direction - Constant stratospheric background wind - Constant stratospheric stability
	005: Propagating TD with vertical shear	- PNJ at $\approx$ 40km - TD moves with phase velocity of Rossby wave - Design idealized wind profile - Use wind profile from ECMWF - **Sensitivity analysis** wrt. shape of depression (h_0, a and asymmetry)
	006: Propagating TD with meridional wind	- Run 2D005 with Coriolis force
3D	007: Propagating TD with vertical shear	- Run 2D005/006 in 3D - TD oriented N-S - Compare elongated and local depression (elliptic shape)
	008: Tilted TD with vertical shear	- Run 3D007 with tilted TD (oriented NW-SE)
	009: Barocl. (or barotropic) PNJ above TD	- Include horizontal shear - 2D Gaussian distribution (for barocl. jet) - θ_{env} from thermal wind relation (for barocl. jet) - PNJ directly above tropopause depression
	010: Barocl. (or barotropic) PNJ shifted south	- Simulation 3D009 with PNJ shifted south
	011: Full simulation including troposphere	- Initialisation based on Bush et al. (1994) - Extension of barocl. instability with PNJ

ously, because the relative speed of the depression with respect to the constant background wind changes, too. In particular, the varying tilt of the phase lines should be observable.

3.2. 2D simulations of a propagating tropopause depression

The next step in the two-dimensional space is the introduction of a realistic stratospheric wind profile (simulation 2D005 in table 1). Two approaches are possible. The first one incorporates the design of idealized profiles with increasing complexity. At first, a PNJ could be represented by a Gaussian distribution peaking at a level between 40-50 km. In a next step, it could be of interest to add a second jet at the tropopause level resulting in a negative wind shear in the lower stratosphere before the wind increases again higher up. For this purpose, a higher order function approximation might be more suited than a superposition of two Gaussian distributions to avoid sharp changes in the vertical shear. Environmental profiles of θ, T or p still refer to a constant stability and an isothermal atmosphere. The second approach relies on realistic ECMWF wind profiles, which are already available from the observational analysis of RF25 of the DEEPWAVE campaign (Dörnbrack et al., 2021). These profiles represent meridional means of a relevant 5° wide latitude band and naturally include complex shear scenarios due to the PNJ and the tropopause jet stream.

For these simulations (2D005) it is planned to reduce the movement of the TD to a constant propagation from left to right through the simulation domain. In this way, the effect of vertical wind profiles on the excitation and propagation of waves above a transient TD is not disturbed by an unrealistic movement of the depression. At the upper and lateral boundaries, the vertical and horizontal radiation of wave energy is treated by relaxation terms as further described in section 4. The parameters of these damping layers are tuned to reduce boundary effects like wave reflection to a minimum.

At this point, it is also planned to conduct a sensitivity analysis with respect to the depression's shape. Effects of its depth, width and possibly asymmetry shall be investigated. The settings used by Prusa and Smolarkiewicz (2003) serve as a good starting point, but observations (Bush and Peltier, 1994 and Keyser and Shapiro, 1986) and reanalysis data (Dörnbrack et al., 2021 and Škerlak et al., 2015) suggest quite a range of realistic parameters. This sensitivity analysis can provide first hints on expected wave regimes and help to identify optimal settings for further simulations.

Simulation 2D006 is closely related to 2D005 with the difference of activating the Coriolis force and allowing meridional winds. All other settings will be left unchanged with respect to a reference simulation of 2D005 to directly observe differences in the wave excitation and propagation.

3.3. 3D simulations of a propagating TD

The first three-dimensional simulations are extending simulations 2D005 and 2D006 into the meridional dimension with a focus on the shape of the TD. As described in section 2.4, two mechanisms are able to describe the meridional propagation of GWs into the PNJ at 60°S. A non-parallel wave vector with respect to the background zonal wind and horizontal wind shear. Neglecting horizontal wind shear for simulations 3D007 and 3D008 allows the isolated investigation of a meridional propagation due to the orientation of the wave vector. In that manner, it is the goal to compare differences in wave propagation between an elongated N-S oriented depression, a N-S oriented, local depression (elliptic shape) and a tilted (NW-SE), local depression (simulation 3D008). The background wind for simulations 3D007 and 3D008 will be the same as in 2D005 and constant in meridional direction. Meridional winds only appear based on the Coriolis force, the environmental V component is zero.

Simulations 3D009 and 3D010 are addressing the second mechanism for horizontal wave propagation, the horizontal wind shear. In addition to the vertical wind shear, it is now the goal to design a baroclinic jet system with vertical and horizontal shear. Thus, the environmental U component varies in horizontal and vertical direction, while the background meridional wind V is still zero. Most likely, a reasonable wind field can be obtained by a

two-dimensional Gaussian distribution. Simulation 3D009 is then planned to have the PNJ directly above the tropopause depression to provide a reference simulation for simulation 3D010 that finally has a baroclinic PNJ south of the tropopause depression.

When introducing a baroclinic jet with horizontal and vertical wind shear as a background (environmental) wind field, its influence on the environmental state of the atmosphere has to be considered. The potential temperature distribution now has to balance the gradients in the wind field on the basis of the thermal wind relation

$$\frac{\partial U}{\partial z} = -\frac{g}{\theta_0 f}\frac{\partial \theta}{\partial y} \tag{6}$$

with g and f being the gravitational acceleration and Coriolis parameter and θ_0 a constant basic state reference temperature. In the case of an isothermal stratosphere the pressure and density fields are fully defined, but further options might be investigated.

An additional simplification for 3D009 and 3D010 could be a barotropic jet with horizontal shear only instead of a baroclinic PNJ. Vertical wind shear would be zero, but the PNJ can still be positioned above the TD (3D009) and further to the south (3D010) to observe differences in the wave propagation with respect to the horizontal gradient in the wind.

3.4. Full simulation including troposphere

Though this final simulation (3D011) of the troposphere and stratosphere is most likely not covered within the proposed thesis, it is still mentioned at this point for the sake of completeness. It comprises the simulation of a baroclinic instability at the tropopause, as already carried out by Bush and Peltier (1994), with the crucial difference of a PNJ in the upper stratosphere to the south. Though Bush and Peltier (1994) cover all relevant equations to define a balanced field that allows the initialisation of a baroclinic jet simulation, it is far from trivial to additionally consider a PNJ.

4. The EULAG numerical solver

The nonlinear numerical simulations are conducted with the EUlerian/semi- LAGrangian fluid solver (EULAG). The model is set up solving the soundproof anelastic set of equations (Lipps and Hemler, 1982) consisting of the three components of the momentum equation (7), the thermodynamic equation (8) for the potential temperature perturbation θ'$=\theta-\theta_e$ and the mass continuity equation (9):

$$\frac{d\vec{v}}{dt} = -G\vec{\nabla}(\frac{p'}{\bar{\rho}}) + \vec{g}\frac{\theta'}{\bar{\theta}} - 2\vec{\Omega}\times(\vec{v}-\vec{v_e}) \\ -\tilde{\alpha}(\vec{v}-\vec{v_e}) \equiv R^v, \tag{7}$$

$$\frac{d\theta'}{dt} = -\vec{v}\cdot\vec{\nabla}\theta_e - \tilde{\beta}(\theta-\theta_e) \equiv R^\theta, \tag{8}$$

$$\vec{\nabla}\cdot(\bar{\rho}\vec{v}) = 0. \tag{9}$$

Here, $\frac{d}{dt}$, $\vec{\nabla}$ and $\vec{\nabla}\cdot$ represent the total derivative, the gradient and the divergence respectively. p' is the pressure perturbation with respect to the environmental state, g the gravitational acceleration and $\vec{\Omega}$ the angular velocity of the Earth. The matrix G represents geometric terms, which result from the general, time-dependent coordinate transformation and the symbol R^Ψ stands for the right-hand side of the corresponding equations for the variables $\Psi = (u, v, w, \theta')$.

$$\bar{\theta}(z) = \theta_0\ \exp(-\frac{N^2}{g}z) \tag{10}$$

and the anelastic density

$$\bar{\rho}(z) = \rho_0\ \exp(-\frac{z}{H_\rho}) \tag{11}$$

refer to the hydrostatic reference state around a constant stability profile as introduced by Bacmeister and Schoeberl (1989) with stability $\frac{N^2}{g}$, a density scale height H_ρ that corresponds to a deep atmosphere and ρ_0, θ_0 set to appropriate reference constants. With (10) and (11) being the basic state of equations (7-9), a more general environmental state, which reflects the initial and boundary conditions, enters the equations via the variables with subscript e. In that sense, $\alpha(\vec{v}-\vec{v_e})$ and $\beta(\theta-\theta_e)$ represent relaxation terms, which enable the radiation of wave energy across the model boundaries

and force the solutions at the model boundaries to the prescribed environmental profiles. These ambient states like u_e, ρ_e or θ_e can be time-dependent to replicate transient flow conditions, but are stationary within the scope of this thesis. On the other hand, transient boundaries like a propagating tropopause fold almost demand for time-dependent terrain-following vertical coordinates as introduced by Wedi and Smolarkiewicz (2003), so this option may be considered at a later stage. Furthermore, EULAG is noteworthy for its robust elliptic solver (P. Smolarkiewicz and Margolin, 1993) and generalized coordinate formulation enabling grid adaptivity technology (Prusa et al., 2008, Kühnlein et al., 2012).

As the name suggests, EULAG is capable of solving the equations of motion (7-9) in an Eulerian (flux form) or in a semi-Lagrangian (advective form) mode (P. K. Smolarkiewicz and Margolin, 1997). For the numerical approximation it utilizes a non-oscillatory forward-in-time (NFT) approach compactly formulated as

$$\Psi^{n+1} = LE(\tilde{\Psi}, V^{n+1}, G^n, G^{n+1}) + \frac{1}{2}\Delta t R^{\Psi}|^{n+1} \tag{12}$$

with LE representing the corresponding semi-Lagrangian/Eulerian transport operator. The NFT scheme belongs to the class of second-order-accurate two-time-level algorithms that are build on nonlinear advection techniques (Prusa et al., 2008). These schemes have the property to suppress and control numerical oscillations that are often found in higher order linear schemes. As a result, transporting the auxiliary field $\tilde{\Psi} = \Psi^n + \frac{1}{2}\Delta t R^{\Psi}|^n$ instead of the specific variable Ψ, results from a thorough truncation error analysis and ensures second order accuracy. (P. K. Smolarkiewicz and Margolin, 1997).

Within the scope of this Master's thesis all simulations utilize the Eulerian option by applying the multidimensional positive definite advection transport algorithm MPDATA (P. K. Smolarkiewicz and Margolin, 1998 and and P. K. Smolarkiewicz, 2006).

EULAG has a proven itself as a reliable tool for simulating thermo-fluid flows across the wide range from turbulent to global scales (Prusa and Smolarkiewicz, 2003) and in a variety of of physical scenarios like e.g. turbulence, GW dynamics, flows past complex/moving boundaries, micrometeorology or cloud microphysics (Prusa et al., 2008). A comparison between different well-established numerical models (including EULAG) and their capability to model flow over steep terrain, which is relevant for the investigations within this thesis, appears in Doyle et al. (2011).

5. Timetable

Figure 4 shall provide a rough overview on individual work packages of the Master's thesis and their allocated time windows. During the first months I had to familiarise myself with the EULAG model and implement a useful baseline for postprocessing and visualizing the EULAG output with Python. In parallel, it was important to undergo a comprehensive literature research, because the thesis tries to address a problem, which has already been investigated from various perspectives. The core of the thesis comprises the simulations and the writing of the manuscript. The goal is to finish all the simulations and a first draft of the thesis by the end of October before I start working for the avalanche warning service in November. Corrections and refinements of the manuscript can be performed throughout the whole winter semester 21/22.

References

Alexander, M. J., Geller, M., McLandress, C., Polavarapu, S., Preusse, P., Sassi, F., Sato, K., Eckermann, S., Ern, M., Hertzog, A., Kawatani, Y., Pulido, M., Shaw, T. A., Sigmond, M., Vincent, R., & Watanabe, S. (2010). Recent developments in gravity-wave effects in climate models and the global distribution of gravity-wave momentum flux from observations and models: Recent Developments in Gravity-Wave Effects. *Quarterly Journal of the Royal Meteorological Society*, *136*(650), 1103–1124. https://doi.org/10.1002/qj.637

Alexander, M. J., Eckermann, S. D., Broutman, D., & Ma, J. (2009). Momentum flux estimates for South Georgia Island mountain waves in the stratosphere observed

Figure 4: Timetable of the proposed Master's thesis

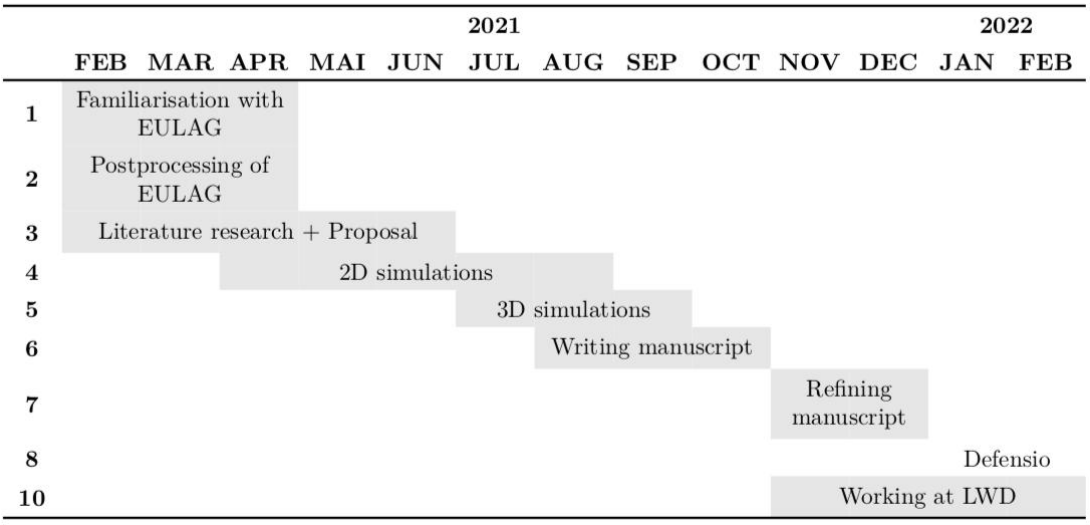

via satellite. *Geophysical Research Letters*, *36*(12), L12816. https://doi.org/10.1029/2009GL038587

Arblaster, J. M., & Meehl, G. A. (2006). Contributions of External Forcings to Southern Annular Mode Trends. *Journal of Climate*, *19*(12), 2896–2905. https://doi.org/10.1175/JCLI3774.1

Bacmeister, J., & Schoeberl, M. (1989). Breakdown of Vertically Propagating Two-Dimensional Gravity Waves Forced by Orography. *Journal of the Atmospheric Sciences*, *46*. https://doi.org/10.1175/1520-0469(1989)046<2109:BOVPTD>2.0.CO;2

Balaji, V. (2015). Climate Computing: The State of Play. *Computing in Science & Engineering*, *17*(6), 9–13. https://doi.org/10.1109/MCSE.2015.109

Balaji, V. (2021). Climbing down Charney's ladder: Machine learning and the post-Dennard era of computational climate science. *Philosophical Transactions of the Royal Society A: Mathematical, Physical and Engineering Sciences*, *379*(2194), 20200085. https://doi.org/10.1098/rsta.2020.0085

Birner, T. (2006). Fine-scale structure of the extratropical tropopause region. *Journal of Geophysical Research*, *111*(D4), D04104. https://doi.org/10.1029/2005JD006301

Birner, T., Dörnbrack, A., & Schumann, U. (2002). How sharp is the tropopause at midlatitudes?: HOW SHARP IS THE TROPOPAUSE AT MIDLATITUDES? *Geophysical Research Letters*, *29*(14), 45–1–45–4. https://doi.org/10.1029/2002GL015142

Bush, A. B. G., & Peltier, W. R. (1994). Tropopause Folds and Synoptic-Scale Baroclinic Wave Life Cycles [Place: Boston MA, USA Publisher: American Meteorological Society]. *Journal of Atmospheric Sciences*, *51*(12), 1581–1604. https://doi.org/10.1175/1520-0469(1994)051<1581:TFASSB>2.0.CO;2

Butchart, N., Charlton-Perez, A. J., Cionni, I., Hardiman, S. C., Haynes, P. H., Krüger, K., Kushner, P. J., Newman, P. A., Osprey, S. M., Perlwitz, J., Sigmond, M., Wang, L., Akiyoshi, H., Austin, J., Bekki, S., Baumgaertner, A., Braesicke, P., Brühl, C., Chipperfield, M., … Yamashita, Y. (2011). Multimodel climate and variability of the stratosphere. *Journal of Geophysical Research*, *116*(D5), D05102. https://doi.org/10.1029/2010JD014995

Chantry, M., Christensen, H., Dueben, P., & Palmer, T. (2021). Opportunities and challenges for machine learning in weather and climate modelling: Hard, medium and soft AI. *Philosophical Transactions of the Royal*

Society A: Mathematical, Physical and Engineering Sciences, *379*(2194), 20200083. https://doi.org/10.1098/rsta.2020.0083

Choi, H.-J., & Chun, H.-Y. (2013). Effects of Convective Gravity Wave Drag in the Southern Hemisphere Winter Stratosphere. *Journal of the Atmospheric Sciences*, *70*(7), 2120–2136. https://doi.org/10.1175/JAS-D-12-0238.1

Dörnbrack, A., Eckermann, S. D., Williams, B. P., & Haggerty, J. A. (2021). Stratospheric gravity waves excited by propagating Rossby wave trains. *Submitted to Journal of Atmospheric Sciences*.

Doyle, J. D., Gaberšek, S., Jiang, Q., Bernardet, L., Brown, J. M., Dörnbrack, A., Filaus, E., Grubišić, V., Kirshbaum, D. J., Knoth, O., Koch, S., Schmidli, J., Stiperski, I., Vosper, S., & Zhong, S. (2011). An Intercomparison of T-REX Mountain-Wave Simulations and Implications for Mesoscale Predictability. *Monthly Weather Review*, *139*(9), 2811–2831. https://doi.org/10.1175/MWR-D-10-05042.1

Dunkerton. (1984). Dunkerton_inertia–Gravity Waves in the Stratosphere. *Journal of Atmospheric Sciences*.

Ehard, B., Kaifler, B., Dörnbrack, A., Preusse, P., Eckermann, S. D., Bramberger, M., Gisinger, S., Kaifler, N., Liley, B., Wagner, J., & Rapp, M. (2017). Horizontal propagation of large-amplitude mountain waves into the polar night jet. *Journal of Geophysical Research: Atmospheres*, *122*(3), 1423–1436. https://doi.org/10.1002/2016JD025621

Eliassen, A., & Palm, E. (1960). On the Transfer of Energy in Stationary Mountain Waves.

Epifanio, C. C., & Durran, D. R. (2001). Three-dimensional effects in high-drag-state flows over long ridges [Publisher: American Meteorological Society]. *Journal of the atmospheric sciences*, *58*(9), 1051–1065.

Eyring, V., Shepherd, T. G., & Waugh, D. W. (2010). *SPARC CCMVal Report on the Evaluation of Chemistry-Climate Models* (tech. rep.) [Backup Publisher: SPARC Publication Title: SPARC Report Volume: No. 5]. SPARC Office. http://www.sparc-climate.org/publications/sparc-reports/

Fritts, D. C. (2003). Gravity wave dynamics and effects in the middle atmosphere. *Reviews of Geophysics*, *41*(1), 1003. https://doi.org/10.1029/2001RG000106

Fritts, D. C., Laughman, B., Wang, L., Lund, T. S., & Collins, R. L. (2018). Gravity Wave Dynamics in a Mesospheric Inversion Layer: 1. Reflection, Trapping, and Instability Dynamics. *Journal of Geophysical Research: Atmospheres*, *123*(2), 626–648. https://doi.org/10.1002/2017JD027440

Fritts, D. C., Smith, R. B., Taylor, M. J., Doyle, J. D., Eckermann, S. D., Dörnbrack, A., Rapp, M., Williams, B. P., Pautet, P.-D., Bossert, K., Criddle, N. R., Reynolds, C. A., Reinecke, P. A., Uddstrom, M., Revell, M. J., Turner, R., Kaifler, B., Wagner, J. S., Mixa, T., ... Ma, J. (2016). The Deep Propagating Gravity Wave Experiment (DEEPWAVE): An Airborne and Ground-Based Exploration of Gravity Wave Propagation and Effects from Their Sources throughout the Lower and Middle Atmosphere. *Bulletin of the American Meteorological Society*, *97*(3), 425–453. https://doi.org/10.1175/BAMS-D-14-00269.1

Garfinkel, C. I., & Oman, L. D. (2018). Effect of Gravity Waves From Small Islands in the Southern Ocean on the Southern Hemisphere Atmospheric Circulation. *Journal of Geophysical Research: Atmospheres*, *123*(3), 1552–1561. https://doi.org/10.1002/2017JD027576

Geller, M. A., Alexander, M. J., Love, P. T., Bacmeister, J., Ern, M., Hertzog, A., Manzini, E., Preusse, P., Sato, K., Scaife, A. A., & Zhou, T. (2013). A Comparison between Gravity Wave Momentum Fluxes in Observations and Climate Models. *Journal of Climate*, *26*(17), 6383–6405. https://doi.org/10.1175/JCLI-D-12-00545.1

Gill, A. E. (1982). *Atmosphere-Ocean Dynamics*. Academic Press.

Hendricks, E. A., Doyle, J. D., Eckermann, S. D., Jiang, Q., & Reinecke, P. A. (2014). What Is the Source of the Stratospheric

Gravity Wave Belt in Austral Winter? *Journal of the Atmospheric Sciences*, *71*(5), 1583–1592. https://doi.org/10.1175/JAS-D-13-0332.1

Hindley, N. P., Wright, C. J., Hoffmann, L., Moffat-Griffin, T., & Mitchell, N. J. (2020). An 18-Year Climatology of Directional Stratospheric Gravity Wave Momentum Flux From 3-D Satellite Observations. *Geophysical Research Letters*, *47*(22). https://doi.org/10.1029/2020GL089557

Hindley, N. P., Wright, C. J., Smith, N. D., Hoffmann, L., Holt, L. A., Alexander, M. J., Moffat-Griffin, T., & Mitchell, N. J. (2019). Gravity waves in the winter stratosphere over the Southern Ocean: High-resolution satellite observations and 3-D spectral analysis. *Atmospheric Chemistry and Physics*, *19*(24), 15377–15414. https://doi.org/10.5194/acp-19-15377-2019

Jewtoukoff, V., Hertzog, A., Plougonven, R., Cámara, A. d. l., & Lott, F. (2015). Comparison of Gravity Waves in the Southern Hemisphere Derived from Balloon Observations and the ECMWF Analyses. *Journal of the Atmospheric Sciences*, *72*(9), 3449–3468. https://doi.org/10.1175/JAS-D-14-0324.1

Jiang, Q., Doyle, J. D., Eckermann, S. D., & Williams, B. P. (2019). Stratospheric Trailing Gravity Waves from New Zealand. *Journal of the Atmospheric Sciences*, *76*(6), 1565–1586. https://doi.org/10.1175/JAS-D-18-0290.1

Kaifler, B., & Kaifler, N. (2021). A Compact Rayleigh Autonomous Lidar (CORAL) for the middle atmosphere. *Atmospheric Measurement Techniques*, *14*(2), 1715–1732. https://doi.org/10.5194/amt-14-1715-2021

Kaifler, N., Kaifler, B., Dörnbrack, A., Rapp, M., Hormaechea, J. L., & de la Torre, A. (2020). Lidar observations of large-amplitude mountain waves in the stratosphere above Tierra del Fuego, Argentina. *Scientific Reports*, *10*(1), 14529. https://doi.org/10.1038/s41598-020-71443-7

Keyser, D., & Shapiro, M. (1986). A Review of the Structure and Dynamics of Upper-Level Frontal Zones. *Monthly Weather Review*, *114*, 452–499.

Kim, Y.-J., Eckermann, S. D., & Chun, H.-Y. (2003). An overview of the past, present and future of gravity-wave drag parametrization for numerical climate and weather prediction models. *Atmosphere-Ocean*, *41*(1), 65–98. https://doi.org/10.3137/ao.410105

Kühnlein, C., Smolarkiewicz, P. K., & Dörnbrack, A. (2012). Modelling atmospheric flows with adaptive moving meshes. *Journal of Computational Physics*, *231*(7), 2741–2763. https://doi.org/10.1016/j.jcp.2011.12.012

Lin, Y.-L. (2007). *Mesoscale Dynamics*. Cambridge University Press. https://doi.org/10.1017/CBO9780511619649

Lipps, F. B., & Hemler, R. S. (1982). A Scale Analysis of Deep Moist Convection and Some Related Numerical Calculations. *Journal of the Atmospheric Sciences*, *39*, 2192–2210.

Matsuoka, D., Watanabe, S., Sato, K., Kawazoe, S., Yu, W., & Easterbrook, S. (2020). Application of Deep Learning to Estimate Atmospheric Gravity Wave Parameters in Reanalysis Data Sets. *Geophysical Research Letters*, *47*(19). https://doi.org/10.1029/2020GL089436

McLandress, C., Shepherd, T. G., Polavarapu, S., & Beagley, S. R. (2012). Is Missing Orographic Gravity Wave Drag near 60°S the Cause of the Stratospheric Zonal Wind Biases in Chemistry–Climate Models? *Journal of the Atmospheric Sciences*, *69*(3), 802–818. https://doi.org/10.1175/JAS-D-11-0159.1

Medvedev, A. S., & Yiğit, E. (2019). Gravity Waves in Planetary Atmospheres: Their Effects and Parameterization in Global Circulation Models. *Atmosphere*, *10*(9), 531. https://doi.org/10.3390/atmos10090531

Metz, J. J., & Durran, D. R. (2021). Are finite-amplitude effects important in non-breaking mountain waves? *Quarterly Journal of the Royal Meteorological Society*, qj.4045. https://doi.org/10.1002/qj.4045

O'Sullivan, D., & Dunkerton, T. J. (1995). Generation of Inertia–Gravity Waves in a Simulated Life Cycle of Baroclinic Instability [Place: Boston MA, USA Publisher: American Meteorological Society]. *Journal of Atmospheric Sciences*, *52*(21), 3695–3716. https://doi.org/10.1175/1520-0469(1995)052<3695:GOIWIA>2.0.CO;2

Pfister, L., Chan, K. R., Bui, T. P., Bowen, S., Legg, M., Gary, B., Kelly, K., Proffitt, M., & Starr, W. (1993). Gravity waves generated by a tropical cyclone during the STEP tropical field program: A case study. *Journal of Geophysical Research: Atmospheres*, *98*(D5), 8611–8638. https://doi.org/10.1029/92JD01679

Plougonven, R., Hertzog, A., & Guez, L. (2013). Gravity waves over Antarctica and the Southern Ocean: Consistent momentum fluxes in mesoscale simulations and stratospheric balloon observations. *Quarterly Journal of the Royal Meteorological Society*, *139*(670), 101–118. https://doi.org/10.1002/qj.1965

Plougonven, R., la Cámara, A., Hertzog, A., & Lott, F. (2020). How does knowledge of atmospheric gravity waves guide their parameterizations? *Quarterly Journal of the Royal Meteorological Society*, *146*(728), 1529–1543. https://doi.org/10.1002/qj.3732

Plougonven, R., & Zhang, F. (2014). Internal gravity waves from atmospheric jets and fronts. *Reviews of Geophysics*, *52*(1), 33–76. https://doi.org/10.1002/2012RG000419

Polichtchouk, I., Shepherd, T. G., Hogan, R. J., & Bechtold, P. (2018). Sensitivity of the Brewer–Dobson Circulation and Polar Vortex Variability to Parameterized Nonorographic Gravity Wave Drag in a High-Resolution Atmospheric Model. *Journal of the Atmospheric Sciences*, *75*(5), 1525–1543. https://doi.org/10.1175/JAS-D-17-0304.1

Preusse, P., Dörnbrack, A., Eckermann, S. D., Riese, M., Schaeler, B., Bacmeister, J. T., Broutman, D., & Grossmann, K. U. (2002). Space-based measurements of stratospheric mountain waves by CRISTA 1. Sensitivity, analysis method, and a case study: STRATOSPHERIC MOUNTAIN WAVE MEASUREMENTS BY CRISTA, 1. *Journal of Geophysical Research: Atmospheres*, *107*(D23), CRI 6–1–CRI 6–23. https://doi.org/10.1029/2001JD000699

Prusa, J. M., & Smolarkiewicz, P. K. (2003). An all-scale anelastic model for geophysical flows: Dynamic grid deformation. *Journal of Computational Physics*, *190*(2), 601–622. https://doi.org/10.1016/S0021-9991(03)00299-7

Prusa, J. M., Smolarkiewicz, P. K., & Wyszogrodzki, A. A. (2008). EULAG, a computational model for multiscale flows. *Computers & Fluids*, *37*(9), 1193–1207. https://doi.org/10.1016/j.compfluid.2007.12.001

Queney, P. (1948). The Problem of Air Flow Over Mountains: A Summary of Theoretical Studies. *Bulletin of the American Meteorological Society*, *29*(1), 16–26. https://doi.org/10.1175/1520-0477-29.1.16

Randel, W. J., Wu, F., & Forster, P. (2007). The Extratropical Tropopause Inversion Layer: Global Observations with GPS Data, and a Radiative Forcing Mechanism. *Journal of the Atmospheric Sciences*, *64*(12), 4489–4496. https://doi.org/10.1175/2007JAS2412.1

Rapp, M., Kaifler, B., Dörnbrack, A., Gisinger, S., Mixa, T., Reichert, R., Kaifler, N., Knobloch, S., Eckert, R., Wildmann, N., Giez, A., Krasauskas, L., Preusse, P., Geldenhuys, M., Riese, M., Woiwode, W., Friedl-Vallon, F., Sinnhuber, B.-M., Torre, A. d. l., … Engel, A. (2021). SOUTHTRAC-GW: An Airborne Field Campaign to Explore Gravity Wave Dynamics at the World's Strongest Hotspot. *Bulletin of the American Meteorological Society*, *102*(4), E871–E893. https://doi.org/10.1175/BAMS-D-20-0034.1

Sato, K., Watanabe, S., Kawatani, Y., Tomikawa, Y., Miyazaki, K., & Takahashi, M. (2009). On the origins of mesospheric gravity waves. *Geophysical Research Letters*, *36*(19), L19801. https://doi.org/10.1029/2009GL039908

Sato, K., Tateno, S., Watanabe, S., & Kawatani, Y. (2012). Gravity Wave Char-

acteristics in the Southern Hemisphere Revealed by a High-Resolution Middle-Atmosphere General Circulation Model. *Journal of the Atmospheric Sciences*, *69*(4), 1378–1396. https://doi.org/10.1175/JAS-D-11-0101.1

Scinocca, J. F. (2003). An Accurate Spectral Nonorographic Gravity Wave Drag Parameterization for General Circulation Models [Place: Boston MA, USA Publisher: American Meteorological Society]. *Journal of the Atmospheric Sciences*, *60*(4), 667–682. https://doi.org/10.1175/1520-0469(2003)060<0667:AASNGW>2.0.CO;2

Scorer, R. S. (1949). Theory of waves in the lee of mountains. *Quarterly Journal of the Royal Meteorological Society*, *75*(323), 41–56. https://doi.org/10.1002/qj.49707532308

Shapiro, M. (1978). Further Evidence of the Mesoscale and Turbulent Structure of Upper Level Jet Stream Frontal Zone Systems. *Monthly Weather Review*, *106*, 1100–1111.

Škerlak, B., Sprenger, M., Pfahl, S., Tyrlis, E., & Wernli, H. (2015). Tropopause folds in ERA-Interim: Global climatology and relation to extreme weather events: TROPOPAUSE FOLDS. *Journal of Geophysical Research: Atmospheres*, *120*(10), 4860–4877. https://doi.org/10.1002/2014JD022787

Smolarkiewicz, P., & Margolin, L. (1993). On Forward-in-Time Differencing for Fluids: Extension to a Curvilinear Framework. *Mon. Weather Rev.*, *121*, 1847–1859. https://doi.org/10.1175/1520-0493(1993)121<1847:OFITDF>2.0.CO;2

Smolarkiewicz, P. K. (2006). Multidimensional positive definite advection transport algorithm: An overview. *International Journal for Numerical Methods in Fluids*, *50*(10), 1123–1144. https://doi.org/https://doi.org/10.1002/fld.1071

Smolarkiewicz, P. K., & Margolin, L. G. (1997). On Forward-in-Time Differencing for Fluids: An Eulerian/Semi-Lagrangian Non-Hydrostatic Model for Stratified Flows. *Atmosphere-Ocean*, *35*(sup1), 127–152. https://doi.org/10.1080/07055900.1997.9687345

Smolarkiewicz, P. K., & Margolin, L. G. (1998). MPDATA: A Finite-Difference Solver for Geophysical Flows. *Journal of Computational Physics*, *140*(2), 459–480. https://doi.org/10.1006/jcph.1998.5901

Stolarski, R. S., Douglass, A. R., Gupta, M., Newman, P. A., Pawson, S., Schoeberl, M. R., & Nielsen, J. E. (2006). An ozone increase in the Antarctic summer stratosphere: A dynamical response to the ozone hole. *Geophysical Research Letters*, *33*(21), L21805. https://doi.org/10.1029/2006GL026820

Teixeira, M. A. C. (2014). The physics of orographic gravity wave drag. *Frontiers in Physics*, *2*. https://doi.org/10.3389/fphy.2014.00043

Wedi, N., & Smolarkiewicz, P. (2003). Extending Gal-Chen and Somerville terrain-following coordinate transformation on time-dependent curvilinear boundaries [Publisher: ECMWF]. https://doi.org/10.21957/2XK2TYVY9

Williams, P. D., Alexander, M. J., Barnes, E. A., Butler, A. H., Davies, H. C., Garfinkel, C. I., Kushnir, Y., Lane, T. P., Lundquist, J. K., Martius, O., Maue, R. N., Peltier, W. R., Sato, K., Scaife, A. A., & Zhang, C. (2017). A Census of Atmospheric Variability From Seconds to Decades. *Geophysical Research Letters*, *44*(21). https://doi.org/10.1002/2017GL075483

WMO. (1957). *Meteorology - A three-dimensional science* (Vol. 6). WMO Bull.

WMO. (1986). *Atmospheric ozone* (Vol. 16). WMO Rep.

Wu, D. L., & Waters, J. W. (1996). Satellite observations of atmospheric variances: A possible indication of gravity waves. *Geophysical Research Letters*, *23*(24), 3631–3634. https://doi.org/10.1029/96GL02907